

Effects of clustering heterogeneity on the spectral density of sparse networks

Tuan Minh Pham,¹ Thomas Peron,² and Fernando L. Metz³

¹*Niels Bohr Institute, University of Copenhagen, Blegdamsvej 17, Copenhagen, 2100-DK, Denmark*

²*Institute of Mathematics and Computer Science, University of São Paulo, São Carlos 13566-590, São Paulo, Brazil*

³*Physics Institute, Federal University of Rio Grande do Sul, 91501-970 Porto Alegre, Brazil*

We derive exact equations for the spectral density of sparse networks with an arbitrary distribution of the number of single edges and triangles per node. These equations enable a systematic investigation of the effect of clustering on the spectral properties of the network adjacency matrix. In the case of heterogeneous networks, we demonstrate that the spectral density becomes more symmetric as the fluctuations in the triangle-degree sequence increase. This phenomenon is explained by the small clustering coefficient of networks with a large variance of the triangle-degree distribution. In the homogeneous case of regular clustered networks, we find that both perturbative and non-perturbative approximations fail to predict the spectral density in the high-connectivity limit. This suggests that traditional large-degree approximations may be ineffective in studying the spectral properties of networks with more complex motifs. Our theoretical results are fully confirmed by numerical diagonalizations of finite adjacency matrices.

I. INTRODUCTION

The adjacency matrix of a network fully encodes its structure, thus providing a great amount of information about dynamical processes on it. This includes the dependence of various critical points on the adjacency matrix's leading eigenvalue, such as the threshold probability for network percolation [1], the critical infection rate for epidemic outbreaks [2, 3], the onset of synchronization of phase oscillators [4], and the linear stability of large dynamical systems, such as neural networks [5] and ecosystems [6]. Structural aspects of networks can also be understood in terms of the spectral properties of the adjacency matrix. For example, the eigenvector centrality is the leading eigenvector of the adjacency matrix [1], while the limits in our capacity to detect communities can be expressed in terms of the network spectra [7, 8]. Hence, to understand both the structural and dynamical properties of a network, it is important to determine the spectrum of its adjacency matrix.

The central question of how the distribution of eigenvalues is affected by a particular network feature, such as the degree heterogeneity, has been studied by an extensive number of works using the so-called configuration model [9–17]. In this model, one generates the degrees from a fixed probability distribution and then randomly connects pairs of nodes to match the prescribed degree sequence. Networks generated through this procedure are locally tree-like, i.e., they contain only long loops of length $O(\ln N)$, where N is the total number of nodes. Although the configuration model allows one to study how degree heterogeneities impact the spectral properties, the absence of short loops makes this model somewhat unrealistic, as real-world networks often exhibit considerable levels of *clustering* [18]. This latter property measures to which extent a triple of nodes form a closed triangle [1].

With the aim of overcoming this limitation of the configuration model, a generative network model with tunable clustering has been introduced independently by Newman [19] and Miller [20]. By generalizing the notion of a degree sequence, each vertex of the Newman-Miller model is attached to a prescribed number of triangles and single edges (i.e., those edges

that do not form triangles). This model has been employed to probe the impact of triangles on the spectral properties of networks [21–24]. In reference [21], using random-matrix techniques, the authors derived approximations for the spectral density of networks with a large average number of triangles. Subsequent studies have developed methods for determining the spectral density of sparse, real-world networks with complex topologies [22–24], including short loops of arbitrary length.

Despite these recent advances, the problem of how the spectral density of *sparse* networks (i.e., those with finite average degree) is influenced by the heterogeneity in the distribution of triangles remains unsolved. In this paper, we approach this problem by deriving a set of exact self-consistent equations for the spectral density that only depend on the network's local structure through the joint distribution of the number of single edges and triangles per node. From a technical viewpoint, our approach generalises the cavity method as developed for Husimi graphs, where single edges are absent [25, 26]. The solutions of our equations yield the full distribution of the diagonal elements of the resolvent. This quantity determines not only the spectral density, but other spectral observables that provide information about the eigenvector statistics [27–29].

We illustrate our method on networks with different distributions of the number of single-edges and triangles. In particular, we show how, for a fixed average number of triangles, fluctuations in the triangle-degree sequence symmetrize the spectral density. This finding is unexpected, given that the skewness of the spectral density depends solely on the number of triangles, the number of edges and the average degree [30]. We show that this phenomenon is a consequence of the decrease in the clustering coefficient as the variance of the triangle distribution increases. In addition, for sufficiently heterogeneous distributions of the number of triangles, the clustering coefficient is no longer a monotonic function of the averaged number of triangles. This implies that the highest clustering does not occur at the maximum average number of triangles, but at an intermediate value.

In the case of regular clustered networks, in which the number of single-edges and triangles is fixed, the spectral density converges to the Wigner law of random matrix theory in the

high-connectivity limit, independently of the number of triangles. In this case, we show that the presence of triangles leads to the failure of both perturbative and non-perturbative approximations for the spectral density in the regime of large mean degrees. Numerical diagonalization results of finite adjacency matrices confirm our theoretical findings.

This paper is organized as follows. In section II, we describe the random clustered network model as introduced in [19, 20]. In section III, we explain in detail how to obtain the resolvent equations by generalizing the standard cavity method to networks with triangles. Section IV presents analytical and numerical results for the spectral density of regular clustered networks and heterogeneous networks. In this section, we also discuss the effects of triangle fluctuations on the spectral density and calculate the clustering coefficient as a function of the variance of the distribution of triangles. We give our final remarks in section IV. The paper contains two appendices. Appendix A explains how to compute the clustering coefficient, while Appendix B presents a detailed account of the population dynamics algorithm.

II. THE RANDOM CLUSTERED NETWORK MODEL

In the Newman-Miller random clustered graph model [19, 20], an undirected graph \mathcal{G} of N nodes is generated from two degree sequences: the sequence $\{s_i\}_{i=1,\dots,N}$ of single-edge degrees, where s_i specifies the number of edges attached to node i that do not belong to triangles; and the sequence $\{t_i\}_{i=1,\dots,N}$, in which t_i is the number of triangles that node i participates in. Accordingly, the total degree of node i is given by $k_i = s_i + 2t_i$, as a triangle contributes with two edges to the total degree of a single node.

A single graph instance is generated by connecting different nodes at random with a uniform distribution, subject to the prescribed degree sequences $\{s_i\}_{i=1,\dots,N}$ and $\{t_i\}_{i=1,\dots,N}$. Since there are two different types of edges in the resulting graph \mathcal{G} , it is convenient to split the local neighbourhood of a node into two different sets. Thus, a given node i is adjacent to a subset $\partial_i^{(s)}$ of nodes that define the single-edge neighbourhood, and to a subset $\partial_i^{(t)}$ of nodes that belong to the triangle-based neighbourhood. More precisely, $\partial_i^{(s)}$ consists of those nodes that are connected to i by single-edges, while $\partial_i^{(t)}$ is formed by the set of 2-tuples $\alpha = \{j_1^{(\alpha)}, j_2^{(\alpha)}\}$ connected to i via triangles. Figure 1(a) depicts the neighbourhoods $\partial_i^{(s)}$ and $\partial_i^{(t)}$ around a given node. The total neighbourhood of i is defined as $\Omega_i \equiv \partial_i^{(s)} \cup \partial_i^{(t)}$.

The ensemble of graphs is completely specified, in the limit $N \rightarrow \infty$, by the joint distribution

$$p_{st} = \lim_{N \rightarrow \infty} \frac{1}{N} \sum_{i=1}^N \delta_{s,s_i} \delta_{t,t_i}, \quad (1)$$

where δ represents the Kronecker symbol. The above quantity provides information about fluctuations in the graph topology, since it gives the fraction of nodes connected to s single-edges

and t triangles. The mean number of single-edges and triangles connected to a node are defined, respectively, by

$$\langle s \rangle = \sum_{s,t=0}^{\infty} s p_{st} \quad \text{and} \quad \langle t \rangle = \sum_{s,t=0}^{\infty} t p_{st}. \quad (2)$$

The corresponding variances, which quantify the fluctuations in the number of single-edges and triangles per node, are obtained from p_{st} as follows

$$\begin{aligned} \sigma_e^2 &= \sum_{s,t=0}^{\infty} (s - \langle s \rangle)^2 p_{st}, \\ \sigma_{\Delta}^2 &= \sum_{s,t=0}^{\infty} (t - \langle t \rangle)^2 p_{st}. \end{aligned} \quad (3)$$

Due to the local constraint $k_i = s_i + 2t_i$, the degree distribution P_k is related to p_{st} as $P_k = \sum_{s,t=0}^{\infty} p_{st} \delta_{k,s+2t}$, while the mean degree c fulfills $c = \langle s \rangle + 2\langle t \rangle$. In what follows, we derive a set of self-consistent equations that determine the spectral density of the ensemble of adjacency matrices generated from this model for an arbitrary distribution p_{st} .

III. THE SPECTRAL DENSITY OF THE ADJACENCY MATRIX

The off-diagonal elements $\{A_{ij}\}_{i,j=1,\dots,N}$ of the $N \times N$ weighted adjacency matrix \mathbf{A} associated to \mathcal{G} store the strength of the symmetric couplings between pairs (i, j) of adjacent nodes. If $A_{ij} = A_{ji} \neq 0$, then there is an undirected edge connecting nodes i and j , whereas $A_{ij} = A_{ji} = 0$ means that i and j do not interact. The diagonal elements of \mathbf{A} are zero. Since there are two types of edges in the network, we assume that the strength of single-edge interactions is given by $A_{ij} = J_e \in \mathbb{R}$, while the weight of the edges belonging to triangles is controlled by $A_{ij} = J_{\Delta} \in \mathbb{R}$. Because $\langle s \rangle$ and $\langle t \rangle$ are finite and independent of N , \mathbf{A} is a sparse random matrix with an average number $\langle s \rangle + 2\langle t \rangle$ of nonzero elements per row or column.

We are interested in the spectral density of the adjacency matrix,

$$\rho(\lambda) = \lim_{N \rightarrow \infty} \frac{1}{N} \sum_{i=1}^N \delta(\lambda - \lambda_i), \quad (4)$$

where $\lambda_1, \dots, \lambda_N$ denotes the set of real eigenvalues of \mathbf{A} . Equation (4) defines the most basic spectral observable in random matrix theory, since it provides the average fraction of eigenvalues around λ . Below we explain how to derive a set of equations for $\rho(\lambda)$.

A. Mapping the problem into a statistical physics calculation

By introducing the $N \times N$ resolvent matrix $\mathbf{G}(z) \equiv (z\mathbf{I} - \mathbf{A})^{-1}$, with \mathbf{I} denoting the identity matrix and $z = \lambda - i\epsilon \in \mathbb{C}$

($\varepsilon > 0$), the spectral density $\rho(\lambda)$ can be expressed in terms of $\mathbf{G}(z)$ via the inverse Stieltjes transform [31]

$$\rho(\lambda) = \lim_{\varepsilon \rightarrow 0^+} \lim_{N \rightarrow \infty} \frac{1}{\pi N} \text{Im Tr } \mathbf{G}(z). \quad (5)$$

Clearly, by computing the diagonal elements $\{G_{ii}(z)\}_{i=1, \dots, N}$ of the resolvent matrix, we are able to reconstruct $\rho(\lambda)$ from the above equation.

To compute the diagonal elements $G_{11}(z), \dots, G_{NN}(z)$, we use the cavity approach as developed in random matrix theory [27, 32]. This method, upon introducing site-dependent real variables $\{x_i\}_{i=1, \dots, N}$ and an associated Hamiltonian

$$H_z(\mathbf{x}) = \frac{i}{2} \sum_{i,j=1}^N x_i (z\mathbf{I} - \mathbf{A})_{ij} x_j, \quad (6)$$

recasts the problem of determining $\rho(\lambda)$ into a statistical mechanics problem of N interacting variables placed at the nodes of \mathcal{G} . In fact, by representing $G_{ii}(z) = (z\mathbf{I} - \mathbf{A})_{ii}^{-1}$ as a Gaussian integral over $\{x_i\}_{i=1, \dots, N}$, we rewrite Eq. (5) as

$$\rho(\lambda) = \lim_{\varepsilon \rightarrow 0^+} \lim_{N \rightarrow \infty} \frac{1}{\pi N} \sum_{k=1}^N \text{Re} \left[\int_{-\infty}^{\infty} \left(\prod_{i=1}^N dx_i \right) x_k^2 \mathcal{P}_z(\mathbf{x}) \right], \quad (7)$$

where we introduced the auxiliary joint distribution

$$\mathcal{P}_z(\mathbf{x}) = \frac{e^{-H_z(\mathbf{x})}}{\int_{-\infty}^{\infty} \left(\prod_{i=1}^N dx_i \right) e^{-H_z(\mathbf{x})}} \quad (8)$$

of $\mathbf{x} = (x_1, \dots, x_N)$. We conclude that the second moments of the local marginals $\mathcal{P}_z(x_k) = \int_{-\infty}^{\infty} \left(\prod_{i=1(\neq k)}^N dx_i \right) \mathcal{P}_z(\mathbf{x})$ ($k = 1, \dots, N$) determine the spectral density by means of Eq. (7).

B. Determining the local marginals with the cavity method

Here we explain how to derive a set of self-consistent equations for the local marginals $\mathcal{P}_z(x_k)$ ($k = 1, \dots, N$). Let $\mathbf{x}_{\mathcal{N}}$ represent the variables $\{x_i\}_{i \in \mathcal{N}}$ on a particular subset \mathcal{N} of nodes. We also define $d\mathbf{x}_{\mathcal{N}} = \prod_{i \in \mathcal{N}} dx_i$ as the integration measure over $\mathbf{x}_{\mathcal{N}}$. In accordance to the partition of Ω_k into $\partial_k^{(s)}$ and $\partial_k^{(t)}$, the graph Hamiltonian $H_z(\mathbf{x})$ can be decomposed as

$$H_z(\mathbf{x}) = \frac{i}{2} \sum_{k=1}^N [z x_k^2 - x_k h_k(\mathbf{x}_{\Omega_k})], \quad (9)$$

where the local field $h_k(\mathbf{x}_{\Omega_k})$ at site k reads

$$h_k(\mathbf{x}_{\Omega_k}) = J_e \sum_{j \in \partial_k^{(s)}} x_j + J_{\Delta} \sum_{\alpha \in \partial_k^{(t)}} \mathbf{x}_{\alpha}^T \mathbf{u}, \quad (10)$$

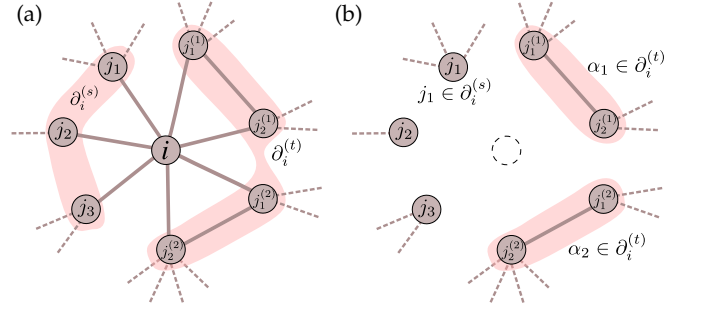


FIG. 1. Illustration of (a) the original graph \mathcal{G} and (b) a cavity graph $\mathcal{G}^{(i)}$, obtained by removing i together with all of its connections from \mathcal{G} in (a). Here the single-edge neighbourhood of i denoted by $\partial_i^{(s)}$ consists of nodes connected to i via single-edges: $\partial_i^{(s)} = \{j_1, j_2, j_3\}$. The triangle neighbourhood of i denoted by $\partial_i^{(t)}$ is the set $\partial_i^{(t)} = \{\alpha_1, \alpha_2\}$, whose elements $\alpha_1 = \{j_1^{(1)}, j_2^{(1)}\}$ and $\alpha_2 = \{j_1^{(2)}, j_2^{(2)}\}$ are the tuples containing nodes connected to i via triangle-edges. Upon removal of i , the nodes j_1, j_2, j_3 and the tuples α_1 and α_2 , all become uncorrelated with each other.

with \mathbf{u} representing the two-dimensional uniform vector $\mathbf{u}^T = (1 \ 1)$. The vector $\mathbf{x}_{\alpha}^T = (x_{j_1}^{(\alpha)}, x_{j_2}^{(\alpha)})$ refers to the pair of variables corresponding to a tuple $\alpha \in \partial_k^{(t)}$. Note that $h_k(\mathbf{x}_{\Omega_k})$ is independent of x_k . Notice also that the graph Hamiltonian in Eq. (9) can be rewritten as

$$H_z(\mathbf{x}) = \frac{i}{2} z x_k^2 - i x_k h_k(\mathbf{x}_{\Omega_k}) + H_z^{(k)}(\mathbf{x}), \quad (11)$$

where the first term on the right-hand side is the contribution of node k to $H_z(\mathbf{x})$, while $H_z^{(k)}(\mathbf{x})$ is the Hamiltonian on the cavity graph $\mathcal{G}^{(k)}$, which is the graph obtained from \mathcal{G} by removing node k and all its edges [see Figure 1(b)]. This allows us to express the marginal distribution $\mathcal{P}_z(x_k)$ as follows

$$\mathcal{P}_z(x_k) \propto e^{-\frac{iz}{2} x_k^2} \int d\mathbf{x}_{\Omega_k} \mathcal{P}^{(k)}(\mathbf{x}_{\Omega_k}) \exp[i x_k h_k(\mathbf{x}_{\Omega_k})], \quad (12)$$

where $\mathcal{P}^{(k)}(\mathbf{x}_{\Omega_k})$ is the joint distribution of \mathbf{x}_{Ω_k} on $\mathcal{G}^{(k)}$. We have ignored an unimportant normalization factor when writing Eq. (12).

The fundamental property that allows us to compute the spectral density using the cavity method is the local tree-like topology of the Newman-Miller model of networks [19, 20]. This property implies that correlations among the neighbours of a given node i are mediated mainly through i [see Figure 1(a)]. After removing the central node i , the neighbourhood Ω_i splits into different subsets of nodes that are essentially disconnected from each other, as illustrated in Figure 1(b). For large N , the typical length of a path that connects two nodes belonging to distinct subsets in Ω_i is of $\mathcal{O}(\ln N)$ [26, 33]. Thus, the nodes $j \in \partial_i^{(s)}$ and the tuples $\alpha \in \partial_i^{(t)}$ become mutually independent on the cavity graph $\mathcal{G}^{(k)}$, yet nodes belonging to the same tuple remain correlated.

Therefore, since the distribution $\mathcal{P}^{(k)}(\mathbf{x}_{\Omega_k})$ is defined on the cavity graph $\mathcal{G}^{(k)}$, the local tree-like structure of \mathcal{G} leads

to the factorization property [34, 35]

$$\mathcal{P}_z^{(k)}(\mathbf{x}_{\Omega_k}) = \prod_{j \in \partial_k^{(s)}} \mathcal{P}_z^{(k)}(x_j) \prod_{\alpha \in \partial_k^{(t)}} \mathcal{P}_z^{(k)}(\mathbf{x}_\alpha). \quad (13)$$

Equation (13) lies at the core of the cavity method since it enables writing $\mathcal{P}_z(x_k)$ in terms of local distributions defined on the cavity graph. Indeed, by substituting Eq. (13) in Eq. (12) and using Eq. (10), we find

$$\begin{aligned} \mathcal{P}_z(x_k) &\propto e^{-\frac{i\mathbf{z}}{2}x_k^2} \prod_{j \in \partial_k^{(s)}} \int_{-\infty}^{\infty} dx_j \mathcal{P}_z^{(k)}(x_j) \exp(iJ_e x_k x_j) \\ &\times \prod_{\alpha \in \partial_k^{(t)}} \int_{-\infty}^{\infty} d\mathbf{x}_\alpha \mathcal{P}_z^{(k)}(\mathbf{x}_\alpha) \exp(iJ_\Delta x_k \mathbf{x}_\alpha^T \mathbf{u}). \end{aligned} \quad (14)$$

Thus, the local marginals $\mathcal{P}_z^{(k)}(x_j)$ and $\mathcal{P}_z^{(k)}(\mathbf{x}_\alpha)$ on the cavity graph determine $\mathcal{P}_z(x_k)$ through the above equation. The rest of the calculation consists of deriving self-consistent equations for $\mathcal{P}_z^{(k)}(x_j)$ and $\mathcal{P}_z^{(k)}(\mathbf{x}_\alpha)$.

The marginal distribution $\mathcal{P}_z^{(k)}(x_j)$ on $\mathcal{G}^{(k)}$, with $k \in \partial_j^{(s)}$, is computed by departing from an expression analogous to Eq. (12), namely

$$\mathcal{P}_z^{(k)}(x_j) \propto e^{-\frac{i\mathbf{z}}{2}x_j^2} \int d\mathbf{x}_{\Omega_j \setminus k} \mathcal{P}_z^{(j,k)}(\mathbf{x}_{\Omega_j \setminus k}) e^{i\mathbf{x}_j^T h_j(\mathbf{x}_{\Omega_j \setminus k})}, \quad (15)$$

in which $\Omega_j \setminus k \equiv (\partial_j^{(s)} \setminus k) \cup \partial_j^{(t)}$ represents the neighbourhood of node j except for $k \in \partial_j^{(s)}$. The distribution $\mathcal{P}_z^{(j,k)}(\mathbf{x}_{\Omega_j \setminus k})$ is defined on a graph $\mathcal{G}^{(j,k)}$ where both nodes, j and $k \in \partial_j^{(s)}$, and all their incident edges are absent. By invoking again the local tree-like topology of the network, one concludes that $\mathcal{P}_z^{(j,k)}(\mathbf{x}_{\Omega_j \setminus k})$ factorizes as follows

$$\mathcal{P}_z^{(j,k)}(\mathbf{x}_{\Omega_j \setminus k}) = \prod_{\ell \in \partial_j^{(s)} \setminus k} \mathcal{P}_z^{(j)}(x_\ell) \prod_{\alpha \in \partial_j^{(t)}} \mathcal{P}_z^{(j)}(\mathbf{x}_\alpha). \quad (16)$$

Note that the local marginals on the right-hand side of the above equation are defined on $\mathcal{G}^{(j)}$ instead of $\mathcal{G}^{(j,k)}$. Indeed, given that the variables on the neighbourhood $\partial_j^{(s)} \setminus k$ are mainly correlated through j , they become independent by simply deleting node j and all its edges. In other words, the removal of the extra node $k \in \partial_j^{(s)}$ is irrelevant for the factorization of $\mathbf{x}_{\partial_j^{(s)} \setminus k}$. This is a crucial step to close the cavity equations and find the expression

$$\begin{aligned} \mathcal{P}_z^{(k)}(x_j) &\propto e^{-\frac{i\mathbf{z}}{2}x_j^2} \prod_{\ell \in \partial_j^{(s)} \setminus k} \int_{-\infty}^{\infty} dx_\ell \mathcal{P}_z^{(j)}(x_\ell) \exp(iJ_e x_j x_\ell) \\ &\times \prod_{\alpha \in \partial_j^{(t)}} \int_{-\infty}^{\infty} d\mathbf{x}_\alpha \mathcal{P}_z^{(j)}(\mathbf{x}_\alpha) \exp(iJ_\Delta x_j \mathbf{x}_\alpha^T \mathbf{u}), \end{aligned} \quad (17)$$

which is obtained by inserting Eq. (16) into Eq. (15).

At last, we need to derive an equation for the local marginal $\mathcal{P}_z^{(k)}(\mathbf{x}_\alpha)$, with $\alpha = \{j_1^{(\alpha)}, j_2^{(\alpha)}\} \in \partial_k^{(t)}$. This is achieved by

considering a graph $\mathcal{G}^{(k,\alpha)}$ obtained from $\mathcal{G}^{(k)}$ by removing the tuple $\alpha = \{j_1, j_2\}$, together with all edges incident to j_1 and j_2 (for simplicity, we have dropped the dependency of $j_1^{(\alpha)}$ and $j_2^{(\alpha)}$ with respect to α). The nodes $\{k, j_1, j_2\}$ form a triangle in the original graph \mathcal{G} . Thus, by repeating the same reasoning as developed above and using the local tree-like topology of the neighbourhoods Ω_{j_1} and Ω_{j_2} , we obtain

$$\begin{aligned} \mathcal{P}_z^{(k)}(\mathbf{x}_\alpha) &\propto \exp\left[-\frac{i\mathbf{z}}{2}(x_{j_1}^2 + x_{j_2}^2) + iJ_\Delta x_{j_1} x_{j_2}\right] \\ &\times \prod_{l \in \partial_{j_1}^{(s)}} \int_{-\infty}^{\infty} dx_l \mathcal{P}_z^{(j_1)}(x_l) \exp(iJ_e x_{j_1} x_l) \\ &\times \prod_{n \in \partial_{j_2}^{(s)}} \int_{-\infty}^{\infty} dx_n \mathcal{P}_z^{(j_2)}(x_n) \exp(iJ_e x_{j_2} x_n) \\ &\times \prod_{\beta \in \partial_{j_1}^{(t)} \setminus \alpha_1} \int_{-\infty}^{\infty} d\mathbf{x}_\beta \mathcal{P}_z^{(j_1)}(\mathbf{x}_\beta) \exp(iJ_\Delta x_{j_1} \mathbf{x}_\beta^T \mathbf{u}) \\ &\times \prod_{\gamma \in \partial_{j_2}^{(t)} \setminus \alpha_2} \int_{-\infty}^{\infty} d\mathbf{x}_\gamma \mathcal{P}_z^{(j_2)}(\mathbf{x}_\gamma) \exp(iJ_\Delta x_{j_2} \mathbf{x}_\gamma^T \mathbf{u}), \end{aligned} \quad (18)$$

with $\alpha_1 = \{j_2, k\}$ and $\alpha_2 = \{j_1, k\}$. Equations (17) and (18) form a closed system of equations for the local marginals $\mathcal{P}_z^{(k)}(x_j)$ and $\mathcal{P}_z^{(k)}(\mathbf{x}_\alpha)$ on the cavity graph $\mathcal{G}^{(k)}$.

Equations (17) and (18) are also known as belief-propagation or message-passing equations [36], since $\mathcal{P}_z^{(k)}(x_j)$ and $\mathcal{P}_z^{(k)}(\mathbf{x}_\alpha)$ can be thought of as representing messages that propagate locally among different regions of the graph. In this context, $\mathcal{P}_z^{(k)}(x_j)$ is a message that propagates from node j to node k through a single-edge, while $\mathcal{P}_z^{(k)}(\mathbf{x}_\alpha)$ is a message that propagates from tuple α to node k by following a pair of edges. The interpretation of Eqs. (17) and (18) as a message-passing algorithm provides a recursive way to efficiently calculate the local marginals on a graph and determine the spectral density for finite $N \gg 1$.

From Eqs. (17) and (18), we can finally derive a set of equations for the diagonal elements $\{G_{kk}(z)\}_{k=1,\dots,N}$ of the resolvent. By inspecting the form of Eqs. (17) and (18), one infers that an appropriate Gaussian *ansatz* for the local marginals solves the cavity equations. We thus assume that the local marginals are given by [27, 32]

$$\mathcal{P}_z(x_k) = \sqrt{\frac{i}{2\pi G_{kk}(z)}} \exp\left(-\frac{i x_k^2}{2G_{kk}(z)}\right), \quad (19)$$

$$\mathcal{P}_z^{(k)}(x_j) = \sqrt{\frac{i}{2\pi G_{jj}^{(k)}(z)}} \exp\left(-\frac{i x_j^2}{2G_{jj}^{(k)}(z)}\right), \quad (20)$$

$$\mathcal{P}_z^{(k)}(\mathbf{x}_\alpha) = \sqrt{\frac{i}{2\pi \det[G_\alpha^{(k)}(z)]}} e^{-\frac{i}{2} \mathbf{x}_\alpha^T \cdot [G_\alpha^{(k)}(z)]^{-1} \mathbf{x}_\alpha}, \quad (21)$$

where $\{G_{jj}(z)\}$ and $\{G_{jj}^{(k)}(z)\}$ are the diagonal elements of the resolvent defined on \mathcal{G} and $\mathcal{G}^{(k)}$, respectively. The 2×2 complex matrix $G_\alpha^{(k)}(z)$ is the resolvent associated to a tuple

$\alpha \in \partial_k^{(t)}$ of the cavity graph $\mathcal{G}^{(k)}$. Substituting the above assumptions in Eqs. (14), (17) and (18), and computing the Gaussian integrals, we find an expression for $G_{kk}(z)$,

$$[G_{kk}(z)]^{-1} = z - J_e^2 \sum_{j \in \partial_k^{(s)}} G_{jj}^{(k)} - J_\Delta^2 \sum_{\alpha \in \partial_k^{(t)}} \mathbf{u}^T \mathbb{G}_\alpha^{(k)} \mathbf{u}, \quad (22)$$

where the cavity resolvents, $\{G_{jj}^{(k)}\}$ and $\{\mathbb{G}_\alpha^{(k)}\}$, solve the self-consistent equations

$$[G_{kk}^{(l)}]^{-1} = z - J_e^2 \sum_{j \in \partial_k^{(s)} \setminus l} G_{jj}^{(k)} - J_\Delta^2 \sum_{\alpha \in \partial_k^{(t)}} \mathbf{u}^T \mathbb{G}_\alpha^{(k)} \mathbf{u}, \quad (23)$$

$$[\mathbb{G}_\alpha^{(k)}]^{-1} = z\mathbb{I} - \mathbb{A} - \mathbb{D}_\alpha^{(k)}, \quad (24)$$

with \mathbb{I} denoting the 2×2 identity matrix. The elements of the two-dimensional matrices \mathbb{A} and $\mathbb{D}_\alpha^{(k)}$ are given by

$$\begin{aligned} (\mathbb{A})_{ij} &= J_\Delta(1 - \delta_{ij}), \\ (\mathbb{D}_\alpha^{(k)})_{ij} &= \delta_{ij} \left(J_\Delta^2 \sum_{\beta \in \partial_j^{(t)} \setminus \alpha_i} \mathbf{u}^T \mathbb{G}_\beta^{(j)} \mathbf{u} + J_e^2 \sum_{l \in \partial_j^{(s)}} G_{ll}^{(j)} \right). \end{aligned}$$

The resolvent Eqs. (22-24) provide an approximation for the spectral density of a single network realization drawn from the Newman-Miller model with a large number N of nodes. Once we obtain a solution of Eqs. (23) and (24), the diagonal elements of the resolvent follow from Eq. (22).

C. The resolvent distributional equations

Equations (22-24) become asymptotically exact as $N \rightarrow \infty$, thanks to the local tree-like topology of the network. In the limit $N \rightarrow \infty$, instead of solving Eqs. (22-24) on a single graph instance, it is sensible to work with an ensemble of random graphs and compute the probability density $W_z(g)$ of the diagonal elements of the resolvent. According to Eq. (5), the spectral density can be written in terms of $W_z(g)$ as

$$\rho(\lambda) = \frac{1}{\pi} \lim_{\epsilon \rightarrow 0^+} \int_{\mathbb{H}^+} dg W_z(g) \text{Im}g, \quad (25)$$

$$W_z(g) = \sum_{s,t=0}^{\infty} p_{st} \int \left(\prod_{\ell=1}^s dg_\ell W_e(g_\ell) \right) \int \left(\prod_{n=1}^t d\mathbb{G}_n W_\Delta(\mathbb{G}_n) \right) \delta \left[g - \left(z - J_e^2 \sum_{\ell=1}^s g_\ell - J_\Delta^2 \sum_{n=1}^t \mathbf{u}^T \mathbb{G}_n \mathbf{u} \right)^{-1} \right] \quad (29)$$

where $W_e(g)$ and $W_\Delta(\mathbb{G})$ follow from the solutions of the self-consistent equations

with $dg = d\text{Re}g d\text{Im}g$. The symbol \mathbb{H}^+ denotes the upper half complex plane. The probability density $W_z(g)$ that a given diagonal element $G_{kk}(z)$ is equal to g reads

$$W_z(g) = \lim_{N \rightarrow \infty} \frac{1}{N} \sum_{k=1}^N \delta[g - G_{kk}(z)], \quad (26)$$

where the Dirac- δ distribution here refers to the complex plane. Likewise, we introduce the probability densities $W_e(g)$ and $W_\Delta(\mathbb{G})$ of the resolvents $G_{jj}^{(k)}$ and $\mathbb{G}_\alpha^{(k)}$, respectively. Such empirical distributions are formally defined as

$$W_e(g) = \lim_{N \rightarrow \infty} \frac{\sum_{j=1}^N \sum_{i \in \partial_j^{(s)}} \delta(g - G_{jj}^{(i)})}{\sum_{i=1}^N s_i} \quad (27)$$

and

$$W_\Delta(\mathbb{G}) = \lim_{N \rightarrow \infty} \frac{\sum_{i=1}^N \sum_{\alpha \in \partial_i^{(t)}} \delta(\mathbb{G} - \mathbb{G}_\alpha^{(i)})}{\sum_{i=1}^N t_i}. \quad (28)$$

The normalization factors in the above equations are related to the total number N_e of edges and to the total number N_Δ of triangles as $N_e = \frac{1}{2} \sum_{i=1}^N s_i$ and $N_\Delta = \frac{1}{3} \sum_{i=1}^N t_i$. Note that $W_e(g)$ and $W_\Delta(\mathbb{G})$ depend on $z \in \mathbb{C}$, but we have omitted such dependency for the sake of simplifying the notation.

Our aim is to derive a set of self-consistent equations that determine $W_z(g)$ and, consequently, the spectral density $\rho(\lambda)$. There are two ways of obtaining such equations, either by inserting Eqs. (22-24) into the Dirac- δ distributions of the above definitions and then computing the ensemble averages, or by simply inspecting what network features control the statistics of the resolvents and then requiring self-consistency, as dictated by Eqs. (22-24). Here we follow the second approach, which is rooted in the fact that the two sides of each one of Eqs. (22-24) must be equal in a distributional sense.

The statistics of $G_{jj}^{(i)}$, $G_{jj}^{(i)}$ and $\mathbb{G}_\alpha^{(i)}$ is determined by the probability p_{st} that a node has s single edges and t tuples. The resolvent $G_{jj}^{(i)}$ is a single-node quantity that depends on p_{st} . The distribution of the single-edge resolvent $G_{jj}^{(i)}$ is determined by the probability $sp_{st}/\langle s \rangle$ that a single edge connects a node attached to s single-edges and t tuples. Finally, $\mathbb{G}_\alpha^{(i)}$ is a triangle-edge quantity which depends on the probability $t_1 t_2 p_{s_1 t_1} p_{s_2 t_2} / \langle t \rangle^2$ to select an edge from a triangle such that one of its nodes is adjacent to (s_1, t_1) and the other to (s_2, t_2) . By requiring that the two sides of each one of Eqs. (22-24) are equal in distribution, we find an expression for the probability density of the resolvent

$$W_e(g) = \sum_{s,t=0}^{\infty} \frac{sp_{st}}{\langle s \rangle} \int \left[\prod_{\ell=1}^{s-1} dg_{\ell} W_e(g_{\ell}) \right] \left[\prod_{n=1}^t d\mathbb{G}_n W_{\Delta}(\mathbb{G}_n) \right] \delta \left[g - \left(z - J_e^2 \sum_{\ell=1}^{s-1} g_{\ell} - J_{\Delta}^2 \sum_{n=1}^t \mathbf{u}^T \mathbb{G}_n \mathbf{u} \right)^{-1} \right], \quad (30)$$

$$W_{\Delta}(\mathbb{G}) = \sum_{s_1, t_1, s_2, t_2=0}^{\infty} \frac{t_1 t_2 p_{s_1 t_1} p_{s_2 t_2}}{\langle t \rangle^2} \int \left[\prod_{\ell=1}^{s_1} dg_{1,\ell} W_e(g_{1,\ell}) \right] \int \left[\prod_{\ell=1}^{s_2} dg_{2,\ell} W_e(g_{2,\ell}) \right] \\ \times \int \left[\prod_{n=1}^{t_1-1} d\mathbb{G}_{1,n} W_{\Delta}(\mathbb{G}_{1,n}) \right] \int \left[\prod_{n=1}^{t_2-1} d\mathbb{G}_{2,n} W_{\Delta}(\mathbb{G}_{2,n}) \right] \delta \left[\mathbb{G} - (z\mathbb{I} - \mathbb{A} - \mathbb{D})^{-1} \right], \quad (31)$$

with the two-dimensional matrix \mathbb{D} defined as

$$(\mathbb{D})_{ij} = \delta_{ij} \left(J_e^2 \sum_{\ell=1}^{s_i} g_{i,\ell} + J_{\Delta}^2 \sum_{n=1}^{t_i-1} \mathbf{u}^T \mathbb{G}_{i,n} \mathbf{u} \right). \quad (32)$$

For the sake of simplicity, we have omitted the dependency of \mathbb{D} in Eq. (31) with respect to the integration variables.

Equations (29-31) make up the main analytic result of this work, since the solutions for $W_z(g)$ determine the spectral density of the Newman-Miller model in the limit $N \rightarrow \infty$ (see Eq. (25)). In the next section, we use the population dynamics algorithm [27, 32] to sample the different terms appearing on the right-hand side of Eqs. (29-31) and iteratively solve these equations. A detailed account of the population dynamics algorithm is presented in appendix B.

IV. RESULTS

In the previous section, we obtained the resolvent distributional Eqs. (29-31) for the spectral density $\rho(\lambda)$ of clustered networks with an arbitrary distribution p_{st} of single-edges and triangles. Here we use those equations to study $\rho(\lambda)$ in two particular cases: random regular clustered graphs and networks with heterogeneous distributions of triangles.

A. Random regular clustered networks

If every node has exactly $\langle s \rangle$ single-edges and $\langle t \rangle$ triangle-edges, then $p_{st} = \delta_{s,\langle s \rangle} \delta_{t,\langle t \rangle}$. In this case, the network becomes homogeneous and the solutions of Eqs. (29-31) read

$$\begin{aligned} W_z(g) &= \delta(g - G), \\ W_e(g) &= \delta(g - G_e), \\ W_{\Delta}(\mathbb{G}) &= \delta(\mathbb{G} - \mathbb{G}_{\Delta}). \end{aligned} \quad (33)$$

By inserting the above expressions into Eqs. (29-31), we conclude that G , G_e and \mathbb{G}_{Δ} fulfill the algebraic equations

$$G^{-1} = z - \langle s \rangle J_e^2 G_e - \langle t \rangle J_{\Delta}^2 \mathbb{G}_{\Delta}, \quad (34)$$

$$G_e^{-1} = z - (\langle s \rangle - 1) J_e^2 G_e - \langle t \rangle J_{\Delta}^2 \mathbb{G}_{\Delta}, \quad (35)$$

$$2\mathbb{G}_{\Delta}^{-1} = z - (\langle t \rangle - 1) J_{\Delta}^2 \mathbb{G}_{\Delta} - \langle s \rangle J_e^2 G_e - J_{\Delta}, \quad (36)$$

where we introduced the scalar quantity $G_{\Delta} = \mathbf{u}^T \mathbb{G}_{\Delta} \mathbf{u}$. The solutions of the above equations determine the spectral density

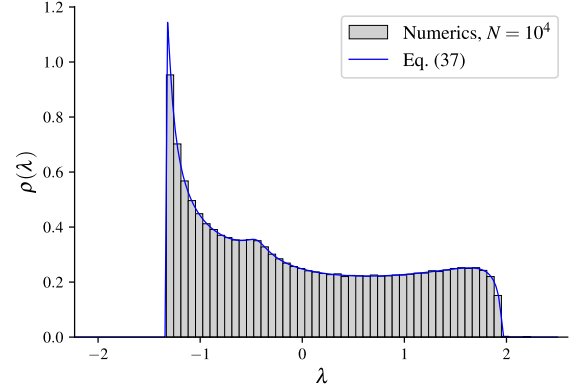


FIG. 2. The spectral density $\rho(\lambda)$ of a random regular clustered network with $\langle s \rangle = 1$ single-edges and $\langle t \rangle = 2$ triangles. The weights of the two different types of edges are $J_e = J_{\Delta} = 1$. The solid line depicts the theoretical result obtained by solving the quartic Eq. (37) for G_{Δ} . The histogram is constructed by numerically diagonalizing the adjacency matrix of a single network realization with $N = 10^4$ nodes.

through Eq. (25). Equations (34-36) admit simple analytic solutions in a few particular cases. The Kesten-McKay law for $\rho(\lambda)$ follows by setting $\langle t \rangle = 0$ in the above equations [26]. For $\langle s \rangle = 0$ and small values of $\langle t \rangle$, we recover the analytic expressions for the spectral density of Husimi networks [25, 26], while the analytic result in [22] is obtained by setting $\langle s \rangle = \langle t \rangle = 1$.

Let us now present results for $\rho(\lambda)$ obtained from the numerical solutions of Eqs. (34-36). For simplicity, we consider $J_{\Delta} = J_e = 1$. Solving Eq. (35) for G_e and then substituting the obtained expression into Eq. (36) yields a quartic equation for G_{Δ} ,

$$[1 - \langle t \rangle - \langle s \rangle] (\langle t \rangle - 1) G_{\Delta}^4 + a_3 G_{\Delta}^3 + a_2 G_{\Delta}^2 + a_1 G_{\Delta} + 4(\langle s \rangle - 1) = 0, \quad (37)$$

where the coefficients are given by

$$\begin{aligned} a_3 &= (\langle t \rangle + z)(\langle s \rangle - 2) + 2\langle t \rangle z - 2(\langle s \rangle - 1), \\ a_2 &= (\langle s \rangle - 2)[\langle s \rangle + 2(\langle t \rangle - 1)] - [(z + \langle s \rangle) - 1](z - 1), \\ a_1 &= -2[z\langle s \rangle + 2(1 - (z + \langle s \rangle))]. \end{aligned} \quad (38)$$

Hence, by solving Eq. (37) and inserting the result in Eqs. (35) and (34), one gets the spectral density from $\rho(\lambda) = (1/\pi) \lim_{\epsilon \rightarrow 0^+} \text{Im} G(z)$.

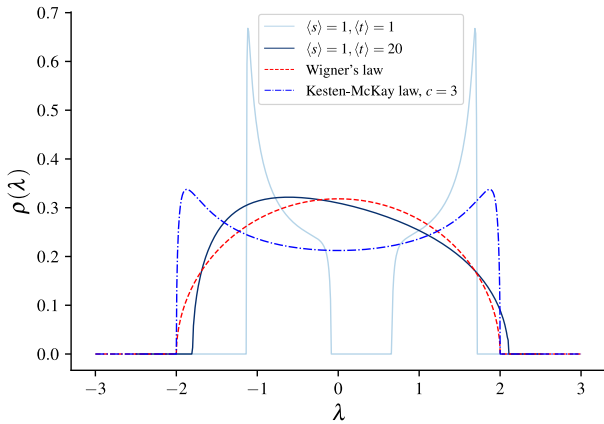


FIG. 3. The spectral density $\rho(\lambda)$ of a random regular clustered network with $\langle s \rangle$ single-edges and $\langle t \rangle$ triangles. The weights of the two different types of edges are $J_e = J_\Delta = 1$. The solid lines show the theoretical results obtained by numerically solving Eqs. (34-36) for different values of $\langle s \rangle$ and $\langle t \rangle$. The dashed line corresponds to the Wigner semicircle law of random matrix theory, which is recovered when the network mean degree is infinitely large. The dash-dotted line is the spectral density of a random regular network in which every node is connected to $\langle s \rangle = 3$ single-edges (Kesten-McKay law).

Figure 2 shows the theoretical curve for $\rho(\lambda)$ obtained from the numerical solution of Eq. (37) for $\langle s \rangle = 1$ and $\langle t \rangle = 2$, along with the histogram of the eigenvalues calculated by numerically diagonalizing the corresponding ensemble of adjacency matrices of regular clustered graphs. The agreement between our theoretical results and numerical diagonalization data is excellent, confirming the exactness of Eqs. (34-36).

In figure 3, we illustrate the shape of the spectral density derived from the solutions of Eq. (37) for different combinations of $\langle t \rangle$ and $\langle s \rangle$. We compare the Kesten-McKay law for locally tree-like networks with degree $c = 3$ and the spectral density of regular clustered networks with $\langle s \rangle = \langle t \rangle = 1$. Although both network models have the same degree $c = 3$, the neighbourhood around each node of the clustered network is coupled by an additional edge. This feature introduces pairwise correlations, which remarkably modify the eigenvalue statistics by inducing a finite gap in the spectral density. In the limit $c \rightarrow \infty$, $\rho(\lambda)$ converges to the Wigner law $\rho_w(\lambda)$ of Gaussian random matrix theory, regardless of the number $\langle t \rangle$ of triangles. Indeed, by setting $J_e = J_\Delta = J/\sqrt{c}$ in Eqs. (34-36) and then taking the limit $c \rightarrow \infty$, we find

$$\rho_w(\lambda) = \frac{\sqrt{\lambda_c^2 - \lambda^2}}{2\pi J^2} \mathbf{1}_{(-|\lambda_c|, |\lambda_c|)}(\lambda), \quad (39)$$

where $|\lambda_c| = 2J$ is the spectral edge. The indicator function $\mathbf{1}_{(-|\lambda_c|, |\lambda_c|)}(\lambda)$ equals one if $\lambda \in (-|\lambda_c|, |\lambda_c|)$, and zero otherwise. For large c , the functional form of $\rho(\lambda)$ is very close to the Wigner law $\rho_w(\lambda)$, as can be noticed from figure 3. This hints at the possibility of devising approximate schemes for the spectral density in the large-connectivity limit. A standard approximation technique consists in computing corrections to $\rho_w(\lambda)$ in a perturbative way [37]. By setting $J_e = J_\Delta = J/\sqrt{c}$ in Eqs. (34-36) and then expanding

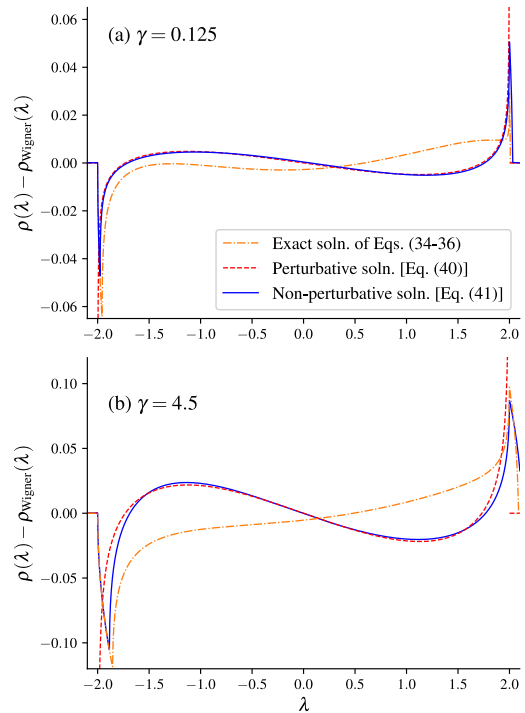


FIG. 4. Deviation of the spectral density $\rho(\lambda)$ of regular clustered graphs with respect to the Wigner law $\rho_w(\lambda)$ for $c = 60$, $J_e = J_\Delta = 1/\sqrt{c}$ and two values of the ratio $\gamma = \langle t \rangle / \langle s \rangle$. The graph compares the exact solution obtained from Eqs. (34-36) with the approximations given by Eqs. (40) and (41). The values of λ that locate the cusps identify the spectral edges obtained from the solutions of the corresponding equations.

$G(z)$ in powers of $1/\sqrt{c}$, we find a perturbative formula for large c ,

$$\rho(\lambda) \simeq \rho_w(\lambda) + \frac{1}{\sqrt{c}} \left[\frac{\gamma}{\pi J^3 (1 + 2\gamma)} \frac{\lambda(\lambda^2 - 3J^2)}{\sqrt{4J^2 - \lambda^2}} \right], \quad (40)$$

with $\gamma = \langle t \rangle / \langle s \rangle$. The above expression provides the leading correction to $\rho(\lambda)$. An alternative non-perturbative approximation for the spectral density can be derived by reducing Eqs. (34-36) to a single cubic equation for the resolvent. This is achieved by setting $J_e = J_\Delta = J/\sqrt{c}$ in Eqs. (34-36) and then neglecting the lowest-order contributions of $\mathcal{O}(1/c)$, which yields the resolvent equation

$$\frac{J^3}{(1 + 2\gamma)} G^3 - J(z + J\sqrt{c})G^2 + (z\sqrt{c} + J)G - \sqrt{c} = 0 \quad (41)$$

for large c . The solutions of Eq. (41) recover the Wigner law when $\gamma = 0$. Equations (40) and (41) provide two distinct approximations for the spectral density of highly-connected clustered networks in the presence of triangles ($\gamma > 0$).

Figure 4 compares, for large mean degree c , the spectral density derived from the approximate Eqs. (40) and (41) with the exact result that follows from the solutions of Eqs. (34-36). The main difference between the perturbative and the non-perturbative approaches is that the latter technique provides better approximations for the spectral edges in the presence of

triangles, while the perturbative approach, in contrast, gives the same spectral edges as those of the Wigner law. Despite that, both approximation schemes fail to yield the correct deviation from the Wigner law in the presence of triangles. This suggests that $\rho(\lambda)$ is never given by the non-perturbative solutions of Eq. (41) nor the perturbative formula of Eq. (40), no matter how large we choose c .

B. Heterogeneous networks

Our goal in this section is to investigate how the heterogeneity in the clustering shapes the spectral density of networks. To this end, we consider networks with a joint distribution $p_{st} = p_s^{(b)} p_t^{(b)}$, where the marginal distributions of the number of single-edges and triangles per node are both given by a negative binomial distribution [28, 38]

$$p_s^{(b)} = \frac{\Gamma(\alpha_e + s)}{s! \Gamma(\alpha_e)} \left(\frac{\langle s \rangle}{\alpha_e} \right)^s \left(\frac{\alpha_e}{\alpha_e + \langle s \rangle} \right)^{\alpha_e + s}, \quad (42)$$

$$p_t^{(b)} = \frac{\Gamma(\alpha_\Delta + t)}{t! \Gamma(\alpha_\Delta)} \left(\frac{\langle t \rangle}{\alpha_\Delta} \right)^t \left(\frac{\alpha_\Delta}{\alpha_\Delta + \langle t \rangle} \right)^{\alpha_\Delta + t}, \quad (43)$$

parametrized by the expected values $(\langle s \rangle, \langle t \rangle)$ and by the parameters $(\alpha_e, \alpha_\Delta)$. The latter are related to the variances of $p_e^{(b)}$ and $p_t^{(b)}$ as follows

$$\sigma_e^2 = \langle s \rangle + \frac{\langle s \rangle^2}{\alpha_e}, \quad \sigma_\Delta^2 = \langle t \rangle + \frac{\langle t \rangle^2}{\alpha_\Delta}. \quad (44)$$

We refer to clustering heterogeneity as the fluctuations in the triangle sequence t_1, \dots, t_N , which are controlled by the variance σ_Δ^2 . For $\alpha_\Delta = 1$, $p_t^{(b)}$ becomes the exponential distribution, while in the limit $\alpha_\Delta \rightarrow \infty$ it converges to the Poisson distribution. For $\alpha_\Delta \rightarrow 0$, the variance σ_Δ^2 diverges, and nodes with an unusually high number of triangles emerge in the network. Therefore, by varying a single parameter, α_Δ , we can continuously increase the heterogeneity in the distribution of triangles. The same idea applies to the distribution $p_s^{(b)}$ of the number of single-edges.

For the standard configuration model, it has been recently shown that $\alpha_e = 1$ marks a regime shift in the high-connectivity limit of the spectral density [17, 28]: for $\alpha_e > 1$, $\rho(\lambda)$ is a regular function, whereas it exhibits a divergence at $\lambda = 0$ when $0 < \alpha_e \leq 1$. This singular behaviour of $\rho(\lambda)$ is ultimately caused by the multifractal structure of the eigenvectors around $\lambda = 0$ [39]. Here we shall analyze the impact of triangle (clustering) fluctuations on $\rho(\lambda)$ under similar choices of α_Δ , while keeping the heterogeneity parameter α_e of single-edges fixed.

For heterogeneous networks, it is in general not possible to obtain closed-form solutions for the spectral density. Thus, we numerically calculate $\rho(\lambda)$ by approximating the probability densities $W_z(g)$, $W_e(g)$ and $W_\Delta(\mathbb{G})$ using the population dynamics algorithm, which is explained in Appendix B. In figure 5 we show results for fixed $(\langle s \rangle, \langle t \rangle)$ and three combinations of the heterogeneity parameters $(\alpha_e, \alpha_\Delta)$. In all cases, the

agreement between the population dynamics algorithm and numerical diagonalization results is excellent.

The network in the first example [figure 5(a)] has a doubly Poisson distribution [$\alpha_e, \alpha_\Delta \rightarrow \infty$ in Eqs. (42) and (43)]. Notice that $\rho(\lambda)$ in figure 5(a) is asymmetric, as expected from previous works [21, 22, 25, 26]. However, if $p_s^{(b)}$ follows a Poisson distribution ($\alpha_e \rightarrow \infty$) and we decrease the heterogeneity parameter α_Δ of triangles, we see that $\rho(\lambda)$ becomes significantly less asymmetric [figures 5(b) and 5(c)]. In fact, for $\alpha_\Delta = 0.5$ in panel (c), the asymmetry of $\rho(\lambda)$ is hardly perceptible, even though the network has the same average number of triangles as in panels (a) and (b). Recall that, by decreasing α_Δ , we increase the variance σ_Δ^2 of distribution $p_t^{(b)}$ [Eq. (44)]. Therefore, the results of figure 5 show that fluctuations in the number of triangles attenuate the lack of symmetry in the spectrum of the adjacency matrix.

To better understand the phenomenon observed in Fig. 5, we calculate the clustering coefficient C of networks with a doubly negative binomial distribution $p_{st} = p_s^{(b)} p_t^{(b)}$. The clustering coefficient is defined as [1]

$$C = \frac{3 \times (\text{number of triangles})}{(\text{number of connected triples})} = \frac{3N_\Delta}{N_3}, \quad (45)$$

where a triple denotes three vertices connected by two edges. Following the steps in Appendix A, we obtain C in terms of the network parameters $\alpha_e, \alpha_\Delta, \langle s \rangle$ and $\langle t \rangle$:

$$C = \frac{2\langle t \rangle}{2\langle t \rangle + (\langle s \rangle + 2\langle t \rangle)^2 + \frac{\langle s \rangle^2}{\alpha_e} + \frac{4\langle t \rangle^2}{\alpha_\Delta}}. \quad (46)$$

Notice that for $\alpha_e, \alpha_\Delta \rightarrow 0$, we get $C \rightarrow 0$. On the other hand, when $\alpha_e, \alpha_\Delta \rightarrow \infty$, we recover the result of the doubly Poisson clustered graph [19]. In figure 6(a), we show C as a function of α_Δ for networks with fixed $\alpha_e = 2$ and $\langle s \rangle = \langle t \rangle = 2$. Note that the clustering coefficient C drops as the triangle fluctuations increase ($\alpha_\Delta \rightarrow 0$). This occurs because the number of possible triples diverges with the variance σ_Δ^2 , while the average number of triangles remains constant across different values of α_Δ . Thus, the proportion of triangles decreases as $\alpha_\Delta \rightarrow 0$, which intuitively explains the gradual loss of asymmetry in the spectral density seen in figure 5.

At last, we present results that illustrate how heterogeneous distributions of triangles impact the maximal value of the clustering coefficient in the special case $\alpha_\Delta = \alpha_e = \alpha$. By setting $\alpha_\Delta = \alpha_e = \alpha$ in Eq. (46), one can find the average number of triangles $\langle t \rangle = \langle t \rangle_{\max}$ that gives the maximal clustering coefficient C_{\max} , namely

$$(\langle t \rangle_{\max}, C_{\max}) = \begin{cases} \left(\frac{c}{2} \sqrt{\frac{(1+\alpha)}{2}}, \Sigma(c, \alpha) \right) & \text{for } 0 < \alpha < 1, \\ \left(\frac{c}{2}, \frac{1}{1+c^2+1/\alpha} \right), & \text{for } \alpha \geq 1, \end{cases} \quad (47)$$

where

$$\Sigma(c, \alpha) \equiv \frac{\sqrt{(1+\alpha)/2}}{(1-2c/\alpha)\sqrt{(1+\alpha)/2} + 4c(1+1/\alpha)}.$$

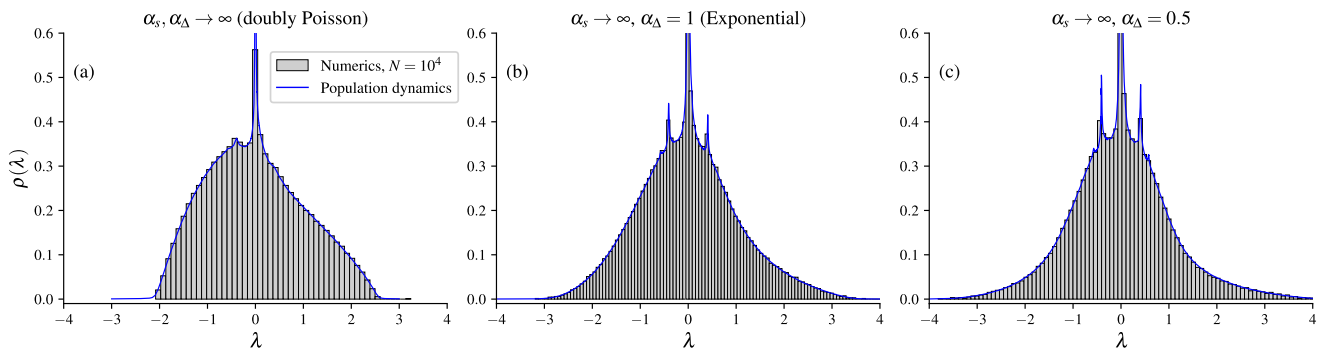


FIG. 5. Spectral density of heterogeneous clustered networks with joint distribution $p_{st} = p_s^{(b)} p_t^{(b)}$ [see Eqs. (42) and (43)] for different combinations of the heterogeneity parameters α_e and α_Δ , whose values are indicated on each panel. All results are obtained for a fixed average number of single edges and triangles ($\langle s \rangle = \langle t \rangle = 2$). In all panels, the solid lines are calculated by solving the set of distributional Eqs. (29-31) using the population dynamics algorithm with $\varepsilon = 0.01$ and a total number of 10^5 stochastic variables (see Appendix A for details). The histograms are obtained by numerically diagonalizing a single realization of the adjacency matrix of a network with $N = 10^4$ nodes, randomly generated from the Newman-Miller model.

For $\alpha \geq 1$, C is a monotonic function of $\langle t \rangle$ and the maximal clustering coefficient is attained when $\langle t \rangle = c/2$, that is, when there are only triangles and no single-edges in the network. Moreover, when $\alpha \rightarrow \infty$, we recover $C_{\max} = 1/(1+c)$, which is the maximum clustering coefficient for doubly Poisson random networks. However, for $\alpha < 1$, C is a non-monotonic function of $\langle t \rangle$, and C_{\max} is reached when the connections are not entirely due to triangles. In other words, for networks with a heterogeneous distribution of triangles, the maximal clustered configuration is obtained for an optimal N_Δ , lower than the total number of possible triangles. This phenomenon is illustrated in figure 6(b), where we show C as a function of $\langle t \rangle$ for $\alpha_\Delta = \alpha_e = \alpha$. Notice that for doubly Poisson ($\alpha \rightarrow \infty$) and exponential ($\alpha = 1$) networks, C_{\max} is obtained at the highest value of the average number of triangles ($\langle t \rangle = 2$). For $\alpha = 0.5$, however, the maximum is found at $\langle t \rangle \simeq 1.75$.

V. DISCUSSION

In this paper, we have used the cavity method to derive a closed set of equations for the spectral density of random clustered networks with an arbitrary joint distribution p_{st} of the number of single-edges and triangles per node. By numerically solving these equations using the population dynamics algorithm, one can exactly compute the spectral density for different choices of the distribution p_{st} in the limit $N \rightarrow \infty$ (N is the total number of nodes). Our theoretical findings are in excellent agreement with numerical diagonalization results for both homogeneous (regular) and heterogeneous *sparse* networks.

For networks with a doubly negative binomial distribution p_{st} , we have shown how increasing fluctuations in the number of triangles reduces the asymmetry of the spectral density. This reduction is a direct consequence of a decrease in the clustering coefficient C as a function of the variance of the number of triangles per node. Interestingly, we have also demonstrated that C reaches a maximum for a number N_Δ of

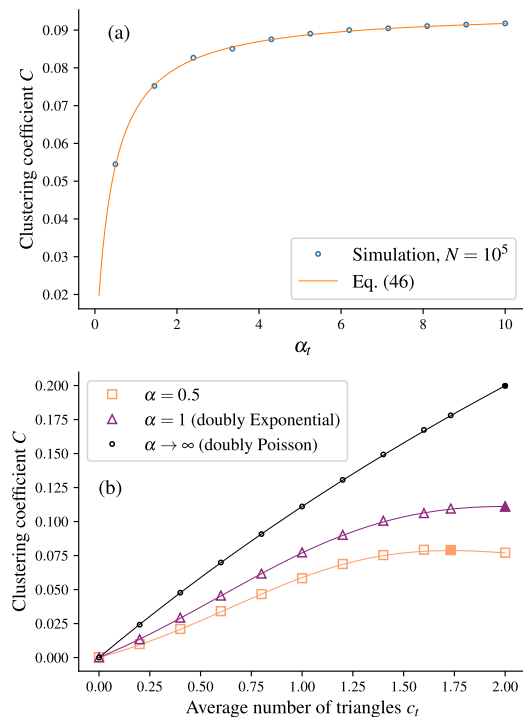


FIG. 6. (a) Clustering coefficient C of networks with doubly negative binomial degree distribution as a function of the heterogeneity parameter α_Δ for fixed $\alpha_e = 2$. The average number of single-edges and triangles is $\langle s \rangle = \langle t \rangle = 2$. Each point is the simulation result of a single randomly generated network with $N = 10^5$ nodes, while the solid line is the theoretical result given by Eq. (46). (b) Clustering coefficient C as a function of the average number of triangles, $\langle t \rangle$, for networks with doubly negative binomial distribution $p_{st} = p_s^{(b)} p_t^{(b)}$ with identical heterogeneity parameters $\alpha_e = \alpha_\Delta = \alpha$ and for fixed average degree $c = 4$. Each point is the simulation result of a single generated network with $N = 10^4$ nodes, and solid lines are analytic results obtained from Eq. (46). Filled dots indicate the analytic predictions [see Eq. (47)] of the points at which the maximal value of C is achieved.

triangles that is lower than the total number of possible triangles in the network.

For regular clustered networks, we have reduced the problem of finding the spectral density to solving a quartic equation. In this case, the spectral density converges to the Wigner law of random matrix theory as the mean degree increases. We have developed a perturbative and a non-perturbative approximation for the spectral density for large mean degrees, but both approximation schemes fail to accurately predict the spectrum. This breakdown of high-connectivity approximations occurs due to the presence of triangles, which might hint at a fundamental difficulty that arises in networks with higher-order structures.

The exactness of our approach relies on the local tree-like property that holds at a larger scale, similar to the cavity approach as applied to Husimi graphs [26]. In principle, our method can be extended to networks composed of higher-order structures, as long as the neighbourhood of each node contains the same species of motifs. Unfortunately, this is often not the case in real-world networks, where our approach is less effective. In this regard, the cavity method is more suitable to study the spectral density of synthetic network models, where the structure of the motifs around each node are known *a priori*.

From a technical perspective, our approach is completely equivalent to the first-order approximation in reference [23], where two neighbors of a node are correlated through a direct link, while all higher-order correlations coming from longer paths connecting these two neighbors are neglected. More specifically, the method of [23] constructs a hierarchy of neighbourhoods around each node and then counts the number of closed walks that initiate and end at this node. The first level of this hierarchical approximation assumes that the network is formed only by single-edges and triangles, which already makes up a very good approximation for real-world networks [23]. In comparison to reference [23], our approach is technically simpler, as it does not involve the complicated combinatorics of counting paths. Besides that, a set of distributional equations for the spectral density can always be obtained by the formulation of the cavity method, as discussed here. These are valid for an ensemble of networks and their solutions do not require a detailed knowledge of the network structure, but only of its statistical properties.

The resolvent equations obtained in our work pave the way to the investigation of the effect of triangle fluctuations on the inverse participation ratio and the local density of states of sparse adjacency matrices [27]. These quantities provide valuable information about the localization properties of eigenvectors. The resolvent equations can also be adapted to compute the spectral density of networks with random weights, which play a central role in the stability analysis of dynamical systems [40]. Finally, it would be interesting to solve Eqs. (29-31) in the high-connectivity limit and probe the universality of the Wigner law with respect to fluctuations in the number of triangles [17, 28]. We hope that our results stimulate further work along these lines.

ACKNOWLEDGMENTS

Tuan Pham acknowledges support from Novo Nordisk Foundation and would like to thank Albert Alonso for stimulating discussions. Thomas Peron acknowledges FAPESP (Grant No. 2023/07481-6) and CNPq/Brazil (Grant No. 310248/2023-0). F. L. M. acknowledges CNPq/Brazil for financial support. This research was carried out using the computational resources of the Center for Mathematical Sciences Applied to Industry (CeMEAI) funded by FAPESP (Grant No. 2013/07375-0).

Appendix A: Clustering coefficient of networks with joint negative binomial degree distribution

In this appendix, we calculate the clustering coefficient for networks with $p_{st} = p_s^{(b)} p_t^{(b)}$, where the marginal distributions of single-edges and triangles are both given by negative binomial distributions

$$p_s^{(b)} = \frac{\Gamma(\alpha_e + s)}{s! \Gamma(\alpha_e)} \left(\frac{\langle s \rangle}{\alpha_e} \right)^s \left(\frac{\alpha_e}{\alpha_e + \langle s \rangle} \right)^{\alpha_e + s}, \quad (\text{A1})$$

$$p_t^{(b)} = \frac{\Gamma(\alpha_\Delta + t)}{t! \Gamma(\alpha_\Delta)} \left(\frac{\langle t \rangle}{\alpha_\Delta} \right)^t \left(\frac{\alpha_\Delta}{\alpha_\Delta + \langle t \rangle} \right)^{\alpha_\Delta + t}, \quad (\text{A2})$$

where $(\langle s \rangle, \langle t \rangle)$ are the expected values of single edges and triangles, respectively, and $(\alpha_e, \alpha_\Delta)$ are the parameters related to the variances of $p_s^{(b)}$ and $p_t^{(b)}$ [see Eq. (44)].

Let us start by writing the generating function of p_{st} :

$$g_p(x, y) = \sum_{s,t=0}^{\infty} p_{st} x^s y^t. \quad (\text{A3})$$

The clustering coefficient is defined as [1]

$$C = \frac{3 \times (\text{number of triangles})}{(\text{number of connected triples})} = \frac{3N_\Delta}{N_3},$$

where a triple denotes three vertices connected by two edges. In terms of g_p , N_Δ and N_3 are written as

$$3N_\Delta = N \sum_{s,t=0}^{\infty} t p_{st} = N \left(\frac{\partial g_p}{\partial y} \right)_{x=y=1}, \quad (\text{A4})$$

and

$$N_3 = N \sum_{k=0}^{\infty} \binom{k}{2} p_k = \frac{1}{2} N \left(\frac{\partial^2 f}{\partial z^2} \right)_{x=y=1}, \quad (\text{A5})$$

where $f(z)$ is the generating function of total degree distribution P_k ,

$$f(z) = \sum_{k=0}^{\infty} P_k z^k = \sum_{s,t=0}^{\infty} p_{st} z^{s+2t} = g_p(z, z^2). \quad (\text{A6})$$

The probability distribution in Eq. (A1) has a generating function given by

$$f_e^{(b)}(z) = \left[\frac{\theta_e}{(1 - (1 - \theta_e)z)} \right]^{\alpha_e}, \quad (\text{A7})$$

where $\theta_e = \alpha_e/(\alpha_e + \langle s \rangle)$. The generating function $f_t^{(b)}(z)$ of $p_t^{(b)}$ is defined analogously to Eq. (A7), but with $\theta_t = \alpha_\Delta/(\alpha_\Delta + \langle t \rangle)$. Hence, $g_p(x, y)$ is written as

$$g_p(x, y) = \left[\frac{\theta_e}{1 - (1 - \theta_s)x} \right]^{\alpha_s} \left[\frac{\theta_t}{1 - (1 - \theta_t)y} \right]^{\alpha_\Delta}, \quad (\text{A8})$$

Substituting Eq. (A8) into Eqs. (A4) and (A5), and inserting the result in Eq. (45), we obtain the clustering coefficient

$$C = \frac{2\langle t \rangle}{2\langle t \rangle + (\langle s \rangle + 2\langle t \rangle)^2 + \frac{\langle s \rangle^2}{\alpha_e} + \frac{4\langle t \rangle^2}{\alpha_\Delta}}. \quad (\text{A9})$$

Appendix B: Algorithm for population dynamics

Algorithm 1 Population dynamics for the calculation of $\rho(\lambda)$ of random graphs with single-edge and triangle degree sequences

Input: eigenvalue λ , regularization parameter ε , population size M , weight of single-edge interactions J_e , weight of triangle interactions J_Δ , marginal distribution of single-edges p_s , marginal distribution of triangles p_t , number of repetitions N_{rep} .

Output: Spectral density $\rho(\lambda)$.

Set p_s as the marginal distribution of single-edges.

Set p_t as the marginal distribution of triangles.

Initialize M variables $g_1, \dots, g_M \in \mathbb{C}$ with positive imaginary parts.

Initialize M two-dimensional matrices $\mathbb{G}_1, \dots, \mathbb{G}_M \in \mathbb{C}$.

repeat

 Draw two random numbers, s_1 and s_2 , from p_s .

 Create two sets, $\partial_1^{(s)}$ and $\partial_2^{(s)}$, with s_1 and s_2 elements, respectively, selected uniformly at random from the indexes $1, \dots, M$.

 Draw two random numbers, t_{e1} and t_{e2} , from $tp_t/\langle t \rangle$.

 Create a set $\partial_1^{(t)}$ of $t_{e1} - 1$ members selected uniformly at random from $1, \dots, M$.

 Create a set $\partial_2^{(t)}$ of $t_{e2} - 1$ members selected uniformly at random from $1, \dots, M$.

$$a_{11} \leftarrow \lambda - i\varepsilon - \left(J_e^2 \sum_{j \in \partial_1^{(s)}} g_j + J_\Delta^2 \sum_{q \in \partial_1^{(t)}} \sum_{i,j=1}^2 [\mathbb{G}_q]_{ij} \right)$$

$$a_{22} \leftarrow \lambda - i\varepsilon - \left(J_e^2 \sum_{j \in \partial_2^{(s)}} g_j + J_\Delta^2 \sum_{q \in \partial_2^{(t)}} \sum_{i,j=1}^2 [\mathbb{G}_q]_{ij} \right)$$

 Select an index $m_1 \in [1, M]$ uniformly at random.

$$\mathbb{G}_{m_1} \leftarrow \begin{pmatrix} a_{11} & -J_\Delta \\ -J_\Delta & a_{22} \end{pmatrix} \quad \triangleright \text{Eq. (24)}$$

 Select an index $m_2 \in [1, M]$ uniformly at random.

 Draw a random number s_{e1} from $sp_s/\langle s \rangle$.

 Create a set $\partial_s^{(3)}$ of $s_{e1} - 1$ members selected uniformly at random from $1, \dots, M$.

 Draw a random number t_1 from p_t .

 Create a set $\partial_t^{(3)}$ of t_1 members selected uniformly at random from $1, \dots, M$.

$$g_{m_2} \leftarrow \left[\lambda - i\varepsilon - \left(J_e^2 \sum_{j \in \partial_s^{(3)}} g_j + J_\Delta^2 \sum_{q \in \partial_t^{(3)}} \sum_{i,j=1}^2 [\mathbb{G}_q]_{ij} \right) \right]^{-1} \quad \triangleright \text{Eq. (23)}$$

until step number $< N_{\text{rep}}$

for $m = 1, \dots, M$ **do**

 Draw a random number s from p_s .

 Draw a random number t from p_t .

 Create a set ∂_s with s elements selected uniformly at random from $1, \dots, M$.

 Create a set ∂_t with t elements selected uniformly at random from $1, \dots, M$.

$$g_m \leftarrow \left[\lambda - i\varepsilon - \left(J_e^2 \sum_{j \in \partial_s} g_j + J_\Delta^2 \sum_{q \in \partial_t} \sum_{i,j=1}^2 [\mathbb{G}_q]_{ij} \right) \right]^{-1} \quad \triangleright \text{Eq. (22)}$$

$$\rho(\lambda) \leftarrow \frac{1}{\pi M} \text{Im} \sum_{j=1}^M g_j$$

return $\rho(\lambda)$

[1] M. Newman, *Networks* (Oxford university press, 2018).

[2] R. Pastor-Satorras, C. Castellano, P. Van Mieghem, and A. Vespignani, Epidemic processes in complex networks, *Reviews of modern physics* **87**, 925 (2015).

[3] G. F. de Arruda, F. A. Rodrigues, and Y. Moreno, Fundamentals of spreading processes in single and multilayer complex networks, *Physics Reports* **756**, 1 (2018).

[4] F. A. Rodrigues, T. K. D. Peron, P. Ji, and J. Kurths, The Kuramoto model in complex networks, *Physics Reports* **610**, 1 (2016).

[5] H. Sompolinsky, A. Crisanti, and H. J. Sommers, Chaos in random neural networks, *Phys. Rev. Lett.* **61**, 259 (1988).

[6] R. M. May, Will a large complex system be stable?, *Nature* **238**, 413 (1972).

- [7] R. R. Nadakuditi and M. E. Newman, Graph spectra and the detectability of community structure in networks, *Physical review letters* **108**, 188701 (2012).
- [8] T. P. Peixoto, Eigenvalue spectra of modular networks, *Physical review letters* **111**, 098701 (2013).
- [9] I. J. Farkas, I. Derényi, A.-L. Barabási, and T. Vicsek, Spectra of “real-world” graphs: Beyond the semicircle law, *Physical Review E* **64**, 026704 (2001).
- [10] F. Chung, L. Lu, and V. Vu, Spectra of random graphs with given expected degrees, *Proceedings of the National Academy of Sciences* **100**, 6313 (2003).
- [11] S. N. Dorogovtsev, A. V. Goltsev, J. F. Mendes, and A. N. Samukhin, Spectra of complex networks, *Physical Review E* **68**, 046109 (2003).
- [12] G. J. Rodgers, K. Austin, B. Kahng, and D. Kim, Eigenvalue spectra of complex networks, *Journal of Physics A: Mathematical and General* **38**, 9431 (2005).
- [13] T. Rogers, C. P. Vicente, K. Takeda, and I. P. Castillo, Spectral density of random graphs with topological constraints, *Journal of Physics A: Mathematical and Theoretical* **43**, 195002 (2010).
- [14] R. Kühn and J. Van Mourik, Spectra of modular and small-world matrices, *Journal of Physics A: Mathematical and Theoretical* **44**, 165205 (2011).
- [15] R. R. Nadakuditi and M. E. Newman, Spectra of random graphs with arbitrary expected degrees, *Physical Review E* **87**, 012803 (2013).
- [16] M. Newman, X. Zhang, and R. R. Nadakuditi, Spectra of random networks with arbitrary degrees, *Physical Review E* **99**, 042309 (2019).
- [17] F. L. Metz and J. D. Silva, Spectral density of dense random networks and the breakdown of the wigner semicircle law, *Phys. Rev. Res.* **2**, 043116 (2020).
- [18] M. E. J. Newman, The structure of scientific collaboration networks, *Proceedings of the National Academy of Sciences* **98**, 404 (2001).
- [19] M. E. J. Newman, Random graphs with clustering, *Phys. Rev. Lett.* **103**, 058701 (2009).
- [20] J. C. Miller, Percolation and epidemics in random clustered networks, *Physical Review E* **80**, 020901 (2009).
- [21] T. K. D. Peron, P. Ji, J. Kurths, and F. A. Rodrigues, Spectra of random networks in the weak clustering regime, *Europhysics Letters* **121**, 68001 (2018).
- [22] M. E. J. Newman, Spectra of networks containing short loops, *Phys. Rev. E* **100**, 012314 (2019).
- [23] G. T. Cantwell and M. E. J. Newman, Message passing on networks with loops, *Proceedings of the National Academy of Sciences* **116**, 23398 (2019).
- [24] G. E. C. Guzman, P. F. Stadler, and A. Fujita, Cavity approach for the approximation of spectral density of graphs with heterogeneous structures, *Phys. Rev. E* **109**, 034303 (2024).
- [25] D. Bollé, F. L. Metz, and I. Neri, On the spectra of large sparse graphs with cycles, *Spectral analysis, differential equations and mathematical physics: a festschrift in honor of Fritz Gesztesy’s 60th birthday*, 35 (2013).
- [26] F. L. Metz, I. Neri, and D. Bollé, Spectra of sparse regular graphs with loops, *Phys. Rev. E* **84**, 055101 (2011).
- [27] F. L. Metz, I. Neri, and D. Bollé, Localization transition in symmetric random matrices, *Physical Review E* **82**, 031135 (2010).
- [28] J. D. Silva and F. L. Metz, Analytic solution of the resolvent equations for heterogeneous random graphs: spectral and localization properties, *Journal of Physics: Complexity* **3**, 045012 (2022).
- [29] D. Tapias and P. Sollich, Multifractality and statistical localization in highly heterogeneous random networks, *Europhysics Letters* **144**, 41001 (2023).
- [30] P. Van Mieghem, *Graph spectra for complex networks* (Cambridge university press, 2023).
- [31] G. Livan, M. Novaes, and P. Vivo, *Introduction to Random Matrices: Theory and Practice*, SpringerBriefs in Mathematical Physics (Springer International Publishing, 2018).
- [32] T. Rogers, I. P. Castillo, R. Kühn, and K. Takeda, Cavity approach to the spectral density of sparse symmetric random matrices, *Phys. Rev. E* **78**, 031116 (2008).
- [33] C. Bordenave and M. Lelarge, Resolvent of large random graphs, *Random Structures & Algorithms* **37**, 332 (2010), <https://onlinelibrary.wiley.com/doi/pdf/10.1002/rsa.20313>.
- [34] R. Kikuchi, A theory of cooperative phenomena, *Phys. Rev.* **81**, 988 (1951).
- [35] J. S. Yedidia, W. T. Freeman, and Y. Weiss, Bethe free energy, Kikuchi approximations, and belief propagation algorithms, *Advances in neural information processing systems* **13**, 689 (2001).
- [36] M. Mézard and A. Montanari, *Information, Physics, and Computation*, Oxford Graduate Texts (OUP Oxford, 2009).
- [37] J. W. Baron, A path integral approach to sparse non-hermitian random matrices (2023), arXiv:2308.13605 [cond-mat.dis-nn].
- [38] F. L. Metz and T. Peron, Mean-field theory of vector spin models on networks with arbitrary degree distributions, *Journal of Physics: Complexity* **3**, 015008 (2022).
- [39] D. Tapias and P. Sollich, Multifractality and statistical localization in highly heterogeneous random networks, *Europhysics Letters* **144**, 41001 (2023).
- [40] A. M. Mambuca, C. Cammarota, and I. Neri, Dynamical systems on large networks with predator-prey interactions are stable and exhibit oscillations, *Phys. Rev. E* **105**, 014305 (2022).